INVESTIGATING PURE, CRYSTALLINE PLAGIOCLASE OUTCROPS EXPOSED ON HUMBOLDT CRATER USING M³ AND DIVINER DATA. M. Martinot[1], K. L. Donaldson Hanna[1], B. T. Greenhagen[2], P. Peplowski[2] and J.T.S. Cahill[2], [1]Department of Physics, University of Central Florida, 4111 Libra Drive, Orlando, FL, USA, [2]Johns Hopkins Applied Physics Laboratory, Laurel, MD, USA (*melissa.martinot@ucf.edu*).

Introduction: Multiple remote sensing surveys have reported the detection of pure, crystalline plagioclase exposures on the central peak of Humboldt crater [1–3] using visible to near infrared (VNIR) data. In this study, the plagioclase-rich regions are investigated using the Moon Mineralogy Mapper (M^3) VNIR hyperspectral data, the global optical maturity (OMAT) index map derived from the Kaguya Multiband Imager (MI) data, and Christiansen feature (CF) maps derived from Lunar Reconnaissance Orbiter (LRO) Diviner multispectral thermal infrared (TIR) data. Our goal is to characterize the maturity, composition (calcium content or An#, calculated as Ca/(Ca+Na)), and homogeneity of plagioclase outcrops exposed on the central peak of Humboldt crater.

Data and Methods: The mineralogy of Humboldt crater was surveyed using VNIR reflectance data from the M³ hyperspectral imager. The M³ instrument orbited the Moon between 2008 and 2009 and obtained data ranging from 0.43 to 3.0 μm [4]. A mosaic of the Humboldt crater was made using OP2C1 Level 2 data from the Planetary Data System (PDS), which have a spatial resolution of 280 m/pixel. PDS Level 2 data are corrected for radiometry [5], geometry [6], thermal [7], and photometry effects [8]. In addition, the ground truth correction developed by [9] was applied. A continuum removal was performed using a technique developed by [3] and similar to that developed by [10].

Band parameters such as integrated band depths of the 1- and 2-micron bands (IBD1000 and IBD2000, respectively) developed by the M³ team [11], and a band parameter developed to highlight crystalline plagioclase occurrences (IBD1250) [12] were used to make color composites highlighting the mineral assemblages exposed on Humboldt crater central peak. A visual inspection of spectra was performed to confirm mineralogical detections, and areas displaying pure, crystalline plagioclase spectra were mapped.

The Kaguya MI derived OMAT global mosaic was utilized to differentiate areas that are optically immature as opposed to mature. Immature regions were defined as areas with OMAT values higher than 0.3. **Figure 1a** shows the map of OMAT variations observed on Humboldt central peak, and the average continuum-removed M^3 spectra for mature and immature regions are shown in **Figure 2**.

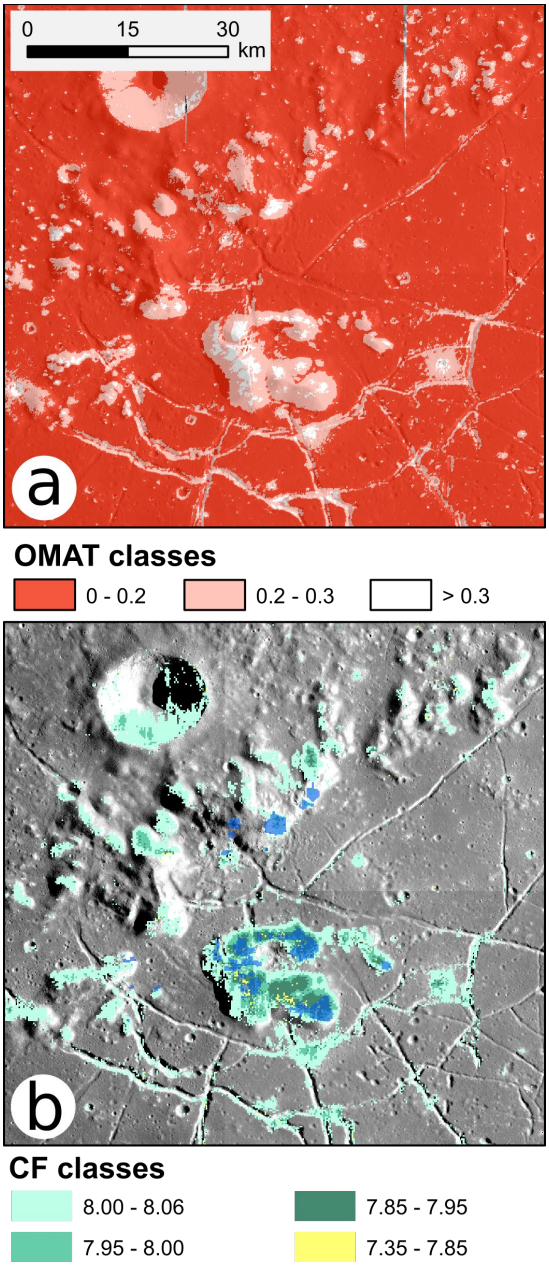

Figure 1: *a) OMAT map of Humboldt crater central peak. Three maturity classes were drawn: an immature class >0.3, an intermediate maturity class between 0.2 and 0.3, and a mature class < 0.2. b) Diviner CF classes overlaid on the LROC Wide Angle Camera (WAC) global mosaic. The blue polygons represent regions identified as pure, crystalline plagioclase exposures with M^3 data.*

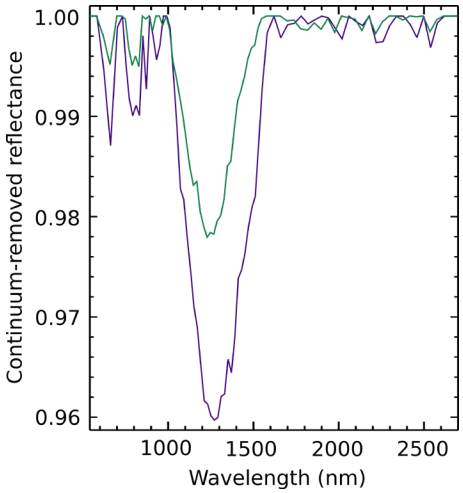

Figure 2: *Continuum-removed M³ spectra of mature areas (in green) and immature areas (in purple).*

Diviner is a nine-channel radiometer onboard LRO, which launched in 2009, and is acquiring data with a spatial resolution of ~200 m [13]. A mosaic of the lunar noontime data (between 10:00 and 14:00) was made over Humboldt crater using Level 3 Diviner data from the PDS. The three TIR channels near 8 µm are used to map the CF position, which varies with changing silicate mineralogy [14]. Pixels with CF positions below 7.35 and above 8.06 µm were masked out, and four classes of CF positions were made and are shown in the **Figure 1b**.

Results: A comparison of average M³ spectra of Humboldt central peak immature and mature regions show plagioclase absorption depths are greater in immature regions. This is consistent with spectral features of fresher, immature material. **Figure 3** shows the median CF positions of immature and mature regions. Both types of regions have similar CF positions regardless of their maturity: mature regions have median CF positions ranging between 7.88 and 8.05 µm, and immature regions have median CF positions ranging between 7.84 and 8.06 µm. Taking a closer look, the median CF position in the linear peak structure to the north of the central peak (outlined in the dashed ellipse in **Figure 3**) span 8.00–8.06 µm, whereas the median CF position in the rest of the central peak span 7.84–8.00 µm.

Discussion and Conclusions: The central peak median CF values are consistent with immature and mature Ca-rich plagioclase compositions [2]. The differences in median CF positions across Humboldt crater central peak need to be investigated further, but may be due to shadowing effects caused by the topography of the central uplift. Alternatively, these differences could be due to differences in alignment

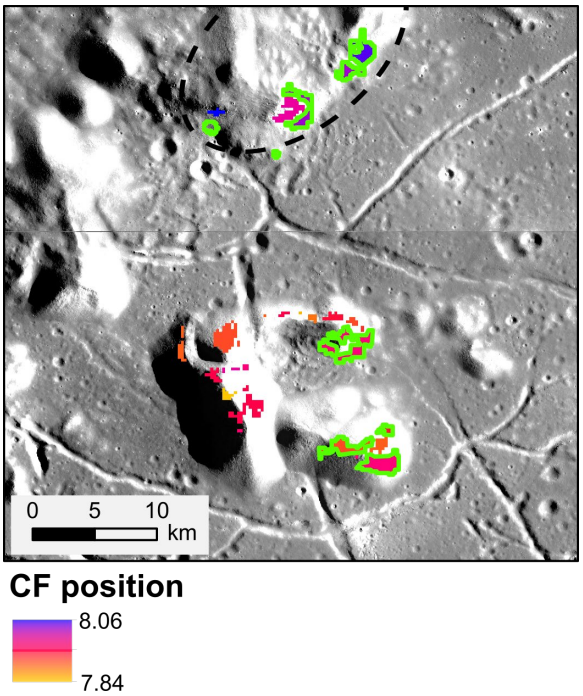

Figure 3: *Median CF position of the pure plagioclase regions on Humboldt crater central peak overlain on the WAC global mosaic. The regions outlined in green represent mature regions, while the other polygons represent immature regions.*

between the LRO datasets and the M³ dataset [15], or differences in spatial resolution between the M³ and the Diviner datasets.

Future work will involve the study of additional datasets such as the optimized Mg# published by [16] to place more constraints on the geochemical suite, since the Mg# is calculated as Mg/(Mg+Fe). More craters will be studied to provide insight into the crustal organization and formation.

Acknowledgments: Martinot, Donaldson Hanna, Greenhagen, Peplowski, and Cahill were funded through the NASA ROSES NNH17ZDA001N-LDAP grant for this work.

References: [1] Yamamoto S. *et al.* (2012) *Geophys. Res. Lett.*, *39*, 1–6. [2] Donaldson Hanna K. L. *et al.* (2014), *JGR Planets*, *119*, 1516–1545. [3] Martinot M., *et al.* (2018), *JGR Planets*, *123*, 612–629. [4] Pieters C. M. *et al.* (2009), *Curr. Sci.*, *96*, 1–6. [5] Green R. O. *et al.* (2011) *JGR Planets*, *116*, 1–31. [6] Boardman J. W. *et al.* (2011), *JGR Planets*, *116*, 1–15. [7] Clark R. N. *et al.* (2011), *JGR Planets*, *116*, 1–9. [8] Besse S. *et al.* (2013), *Icarus*, *222*, 229–242. [9] Isaacson P. J. *et al.* (2013), *JGR Planets, 118*, 369–381. [10] Horgan B. H. N. *et al.* (2014), *Icarus*, *234*, 132–154. [11] Mustard J. F. *et al.* (2011), *JGR Planets*, *116*, 1–17. [12] Cheek L. C. *et al.* (2013), *JGR Planets*, *118*, 1805–1820. [13] Paige D. A. *et al.* (2010) *Space Sci. Rev.*, *150*, 125–160. [14] Greenhagen B. T. (2009), Thesis. [15] Malaret E. *et al.* (2019) *LPSC*, contribution 2132. [16] Crites S. T. and Lucey P. G. (2015) *Am. Mineral.*, *100*, 973–982.